Advanced Course and Workshop on Blood Flow
BF 2005 – (pp.489–500) – Warsaw, 2005.

Estimation of Wall Shear Stress Using a Multi-Branched Model of the Human Arterial System

Pavel V. Stroev[1)], Jason J. Beech-Brandt[1)],
Salikh S. Zakirov[2)] Peter R. Hoskins[3)]
William J. Easson[1)]

[1)] *School of Engineering and Electronics, The University of Edinburgh, Edinburgh, EH9 3JL, Scotland*
Pavel.Stroev@ed.ac.uk

[2)] *Intel, 14 Bolshoy Savvinsky, Moscow, 119435, Russia*

[3)] *Medical Physics Section, The University of Edinburgh, Chancellors Building, 49 Little France Crescent, Edinburgh, EH16 4SB, Scotland*

Simulation of wall shear stress (WSS) is of interest in studies, which attempt to identify the effect of alterations in the geometry and physical properties of the circulation on WSS and on the potential for disease development. Computational fluid dynamics and finite element simulations are computationally demanding, and only model a small section of the arterial system. An alternative approach is the use of a multi-branched model to provide estimates of WSS in different regions throughout the arterial tree.

In the present paper the arterial system was represented by a multi-branched model. Velocity profiles occurring in fully developed pulsatile flow were obtained using Womersley's theory. Mean and peak WSS were calculated in different arteries. Simulations for aging and atherosclerosis were also carried out.

The 1D multi-branched model is easy to implement and it is not computationally demanding. It may be used for detailed quantitative analysis of the velocity profiles obtained by assigning specific values to the various portions of the model of the human arterial tree. It may therefore be a useful tool to estimate WSS in arteries, allowing the effect of alteration of model parameters on WSS to be investigated.

Key words: *Transmission line, systemic circulation, shear rate*

1. Introduction

It is now generally agreed that mechanical and hemodynamic factors are responsible for the development of arterial diseases. It was demonstrated in a number of studies that atherosclerotic plaque is initiated in regions of low or oscillating wall shear stress (WSS) [5, 14, 27]. Simulation of WSS is of interest in studies which attempt to identify the effect of alterations in the geometry and physical properties of the circulation on WSS and on the potential for disease development. Having bifurcations and curved vessels in a complex 3D arterial system leads to complex flow patterns, in which there are commonly secondary flow motions, and in some vessels, such as the carotid, regions of flow recirculation. The usual approach that has been taken in flow simulation is the use of computational fluid dynamics (CFD) [24, 21, 22] and finite element modelling (FEM) [23]. These methods can provide detailed 3D images showing the time varying WSS patterns in particular arteries. However, such simulations are computationally demanding, and only model a small section of the arterial tree.

In this study we used a multi-branched configuration proposed by Avolio [1] reflecting the layout of the human arterial tree. Validation studies of other models based on the same concept [20, 13] have demonstrated a good agreement with experiments and proved to be very robust. The model is an analogue of the uniform transmission line in electrical engineering, which is based on linear theory, thus allowing use of spectral techniques.

We present a simulation, which enables us to explore the effects of various changes in model design, such as the effect of altering characteristics of the arteries and downstream resistance, and to simulate various pathological and physiological conditions. The aim of this study is to obtain such profiles to see whether they give physically realistic estimates of WSS at the different points of the system.

2. Method

WSS, by definition, is $\mu(\nabla \mathbf{u} + \nabla \mathbf{u}^T)$, where μ is dynamic viscosity, and $\nabla \mathbf{u}$ is the velocity gradient (T denotes transposition). For axial flow, WSS becomes $\mu \frac{\partial w}{\partial r}\big|_{r=R}$, where R is the radius of the vessel, and $w(r,t)$ is axial velocity being a function of radius r and time t.

We used Womersley's solution for fully developed pulsatile flow in a straight circular cylinder to obtain velocity profiles as a function of flow rate [23]

rather than pressure gradient [25]. If the inlet length for the k^{th} tube is no less than $0.06R_k\text{Re}$, where $\text{Re} = 2R_k v/\nu$ is Reynolds number, v being average flow velocity, and ν—kinematic viscosity, the radial and circumferential components of velocity and pressure can be overlooked as negligible, pressure varies linearly with axial position, and the axial velocity becomes a function of t and r only [6].

Given the flow rate as the function of time $Q(t)$, in the frequency domain we have the Fourier representation

$$Q(t) = \sum_{n=0}^{N} B_n e^{in\omega t}$$

where N is the number of harmonics, B_n are the coefficients of the Fourier series and ω is the circular frequency.

Now we can find the Womersley velocity profiles:

$$w(r,t) = \frac{2B_0}{\pi {R_k}^2}\left[1 - \left(\frac{r}{R_k}\right)^2\right] + \sum_{n=1}^{N}\left\{\frac{B_n}{\pi {R_k}^2}\left[\frac{1 - \frac{J_0(\alpha_n \frac{r}{R_k} i^{3/2})}{J_0(\alpha_n i^{3/2})}}{1 - \frac{2J_1(\alpha_n i^{3/2})}{\alpha_n i^{3/2} J_0(\alpha_n i^{3/2})}}\right]\right\} e^{in\omega t}$$

where $\alpha_n = R_k\sqrt{\frac{n\omega}{\nu}}$ is the Womersley number, R_k being the radius of the k^{th} artery and ν—kinematic viscosity; J_0 and J_1 are Bessel functions of the first kind of order 0 and 1 respectively.

For the k^{th} vessel of the system, the transfer function relates the distal pressure P_{dk} to the proximal pressure P_{pk} as

$$\frac{P_{dk}}{P_{pk}} = \frac{1 + \Gamma_k}{e^{\gamma_k l_k} + \Gamma_k e^{-\gamma l_k}} \tag{2.1}$$

where l_k is the length of the k^{th} vessel, Γ_k is the reflection coefficient, and γ_k is the propagation constant for the k^{th} artery. The reflection coefficient is expressed as

$$\Gamma_k = \frac{Z_{Tk} - Z_{0k}}{Z_{Tk} + Z_{0k}} \tag{2.2}$$

where Z_{Tk} is the terminal impedance and Z_{0k} is the characteristic impedance of the k^{th} segment of the system, which is expressed as

$$Z_{0k} = \frac{\rho c_{0k}}{\pi {R_k}^2\sqrt{1-\sigma^2}}(1 - F_{10k})^{-1/2} e^{i\phi_k/2}$$

where ρ is density of blood, and the pulse wave velocity for the k^{th} tube is defined by the Moens-Korteweg equation as

$$c_{0k} = \sqrt{\frac{E_k h_k}{2\rho R_k}}$$

where E_k is the value of elastic modulus and h_k is wall thickness of the k^{th} artery, σ is the Poisson ratio, and the Womersley function F_{10k} is defined by

$$F_{10k} = \frac{2J_1(\alpha_k i^{3/2})}{\alpha_k i^{3/2} J_0(\alpha_k i^{3/2})}.$$

The phase difference ϕ between the applied force and the resulting displacement is expressed as $\phi = \phi_0(1 - e^{-2\omega})$, where ϕ_0 is an asymptotic value.

The propagation constant is expressed as

$$\gamma_k = \frac{i\omega}{c_{0k}} \sqrt{\frac{1-\sigma^2}{1-F_{10k}}} e^{-i\phi_k/2}$$

and the input impedance of the k^{th} segment is expressed as

$$Z_{ik} = Z_{0k} \frac{1 + \Gamma_k e^{-2\gamma_k l_k}}{1 - \Gamma_k e^{-2\gamma_k l_k}}. \tag{2.3}$$

If the k^{th} vessel is not a terminal one, there are n vessels branching out of it. In this case,

$$\frac{1}{Z_{Tk}} = \sum_{p=1}^{n} \frac{1}{Z_{ip}} \tag{2.4}$$

where Z_{ip} is input impedance of the p^{th} vessel branching out of the k^{th} vessel.

We assumed all the terminal vessels of the branching structure to be terminated in windkessels with resistance R_k and capacitance C_k [16, 12, 13]. If the k^{th} vessel is a terminal one,

$$Z_{Tk} = Z_{0k} + \frac{1}{\frac{1}{R_k} + i\omega C_k}. \tag{2.5}$$

Terminal impedances of the peripheral branches are obtained using Eq. (2.5). Then their input impedances are worked out with Eq. (2.3). Wherever branching takes place, Eq. (2.4) is used to work out the terminal impedance of the upstream vessel once input impedances of all the downstream vessels

are known. Working backwards towards the origin of the system, the input impedance of every sub-system is obtained. The terminal impedance of the upstream vessel is taken as the input impedance to the downstream sub-system of the vessels and the reflection coefficients are worked out using Eq. (2.2). Equation (2.1) gives the transfer functions—the complex numbers with moduli giving the amount of amplification or attenuation of a particular frequency traveled along the vessel and phase giving the time lag. This gives us pressure waves and, as input impedances are known, flow waves in every artery are also obtained.

2.1. Anatomical Data

Vascular dimensions and elastic constants were taken from [1], except for the upper limbs. It was pointed out in [13] that use of the data given in [1] produced a relatively slow average pulse wave velocity, so corrected data for the upper limbs were introduced in that work and were used in our model also. The values for resistance R and compliance C of the windkessels representing distal terminations were taken from [16]. The flow waveform at the aortic root, which was taken as the input signal to the model, is shown in Fig. 1.

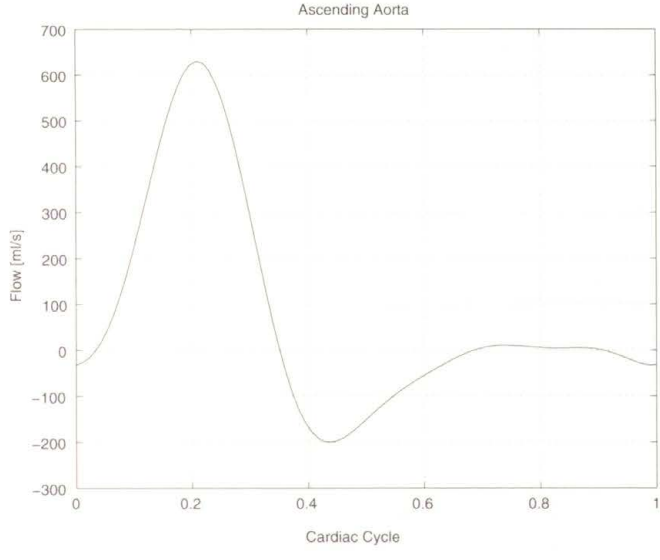

FIGURE 1. Flow rate at the aortic root—input signal to the model

In order to be able to compare the results for the healthy arteries before going on to simulating disease, the following parameters were taken as in [1]: wall viscoelasticity ϕ_0 was taken as 15°, blood viscosity $\mu = 0.004\,\mathrm{Pa\,s}$, blood density $\rho = 1050\,\mathrm{kg/m^3}$, and Poisson ratio $\sigma = 0.5$.

2.2. Simulations

As a demonstration of the model's capability, the following physiological and clinical conditions have been simulated: age-related changes in the elastic properties of the arterial wall and focal atherosclerosis.

The stiffness of arterial segments is known to increase with advancing age [15, 11]. Regional differences in distensibility were noted by many researchers [4, 17], with distensibility being less in abdominal aorta than in thoracic aorta. In the systemic arteries pulse wave velocity shows a greater increase with age in the aorta than in peripheral arteries [2, 10], so we doubled the stiffness of the aorta and used factor 1.5 for all the other arteries to simulate aging.

In simulation of focal atherosclerosis the length of stenosis was somewhat arbitrarily taken as 0.7 cm in the middle of the femoral artery (12.7 cm long). The decrease of the vessel diameter was taken as 80% (severe stenosis). The plaque was taken to be 10 times stiffer than healthy arterial wall. Flow rate and WSS were calculated for both healthy and stenosed artery at the sites A and B shown in Fig. 2.

FIGURE 2. Model of the stenosed artery. Flow rate and WSS were estimated at the points A and B.

3. Results

During the simulations flow rate and WSS have been estimated for some major arteries: brachial, carotid, radial, thoracic aorta, abdominal aorta, common iliac, femoral, popliteal and tibial artery. Peak and average WSS predicted from our model are shown in Table 1.

TABLE 1. Peak and average flow [ml/s] and WSS [Pa] in the arteries.

Artery	Peak Flow	Mean Flow	Peak WSS	Mean WSS
Brachial	10.83	5.32	3.75	1.52
Common carotid	10.76	6.514	1.45	0.65
Radial	3.08	1.618	4.01	2.02
Thoracic aorta	172.4	25.12	3.58	0.14
Abdominal aorta	75.18	13.86	4.69	0.38
Common iliac	23.98	6.05	1.74	0.22
Femoral	9.20	2.53	4.16	0.93
Popliteal	7.91	2.54	5.69	1.6

3.1. Aging

The effects of non-uniform increase of arterial stiffness on blood flow rate and WSS in common carotid artery are shown in Fig. 3.

With advancing age, the reflected wave arrives earlier during ejection and the amplitude of the reflected wave increases causing a decrease in mean volume flow and mean WSS in common carotid artery. When aortic stiffness was doubled and factor 1.5 was used for all the other arteries, we noted 6% decrease in mean volume flow and mean WSS. High frequency oscillations become slightly damped due to the non-uniform increase of arterial stiffness.

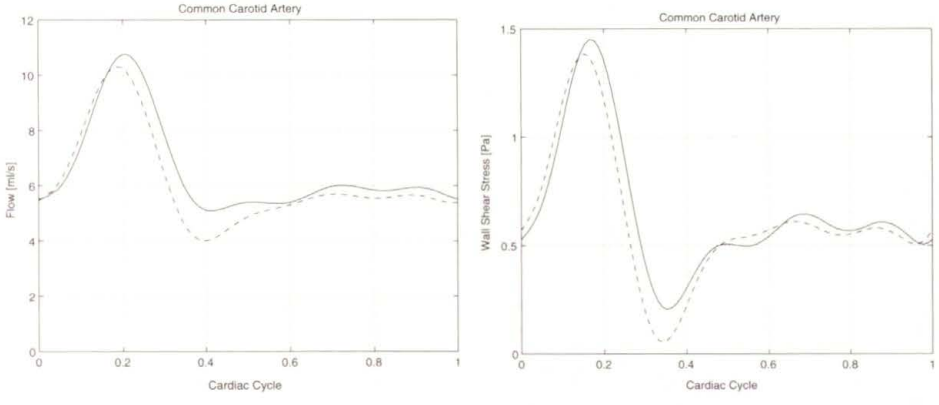

FIGURE 3. Flow rate and WSS in common carotid artery of a younger person (solid line) and those of an older person (broken line).

3.2. Focal Atherosclerosis

Flow rates and WSS in the stenosed femoral artery are shown on Fig. 4 by the solid lines just before the stenosis (site A on Fig. 2) and by the broken lines immediately after it at the site B.

On Fig. 5, the flow rate and WSS in the healthy femoral artery are shown. Solid and broken lines show flow rates and WSS at the same points along the artery. It can be seen that in the case of the stenosed artery phase shift is much more pronounced and the flow wave is attenuated.

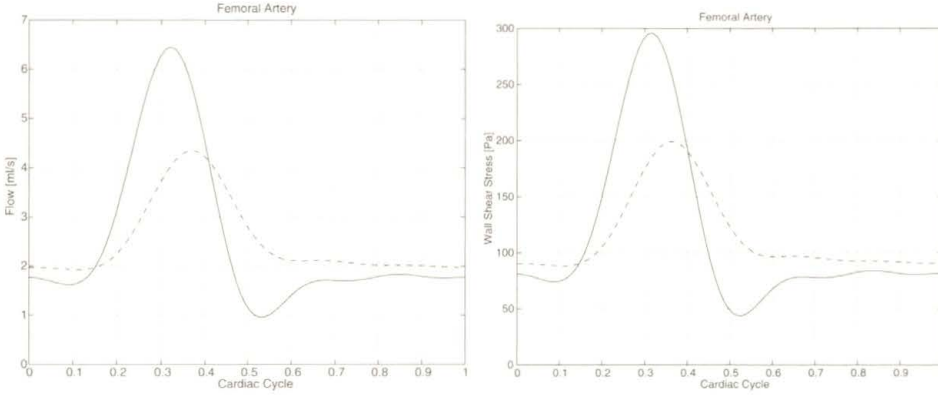

FIGURE 4. Flow rate and WSS in stenosed femoral artery at the points A (solid line) and B (broken line) shown on figure 2.

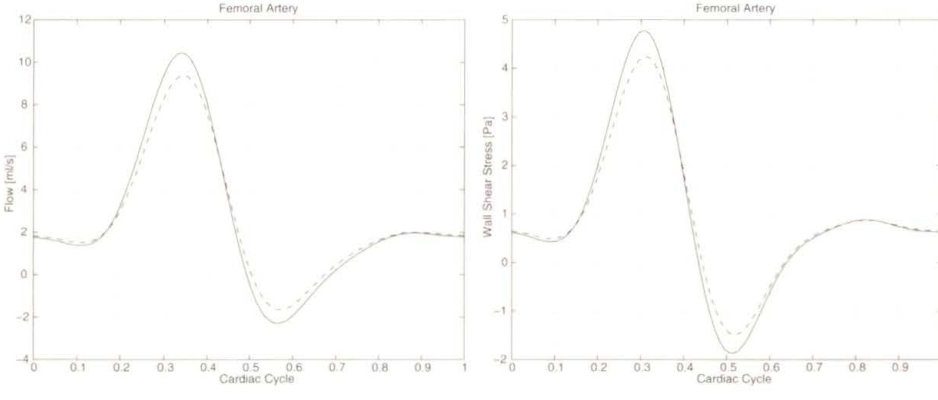

FIGURE 5. Flow rate and WSS in healthy femoral artery at the points A (solid line) and B (broken line) shown on figure 2.

4. Discussion

This study investigates the effects of arterial properties and their interaction with flow wave propagation in the human arterial tree. A distributed model represents the layout of the larger arteries in the systemic circulation. Windkessels represent the lumped or effective properties of the terminations making it possible to account for the effects of altered arterial tone and the capacitance of the small arterioles. In our work, the velocity profiles occurring in fully developed pulsatile flow in the model of the systemic arterial circulation taking account of presence of multiple reflection sites due to branching and tapering were used [20], so physically realistic estimates can be expected.

Local geometry is known to be the main factor determining WSS patterns in the arteries [7]. However, such local differences do not explain the difference in WSS between relatively straight segments in different parts of the arterial tree. The model described in this work can be used to obtain estimates of flow rate and WSS in such segments, as it is reasonable to assume fully developed flow there.

Our estimates for WSS are different to the measurements of wall shear rate reported by Wu et al. [26], who suggested a non-uniform distribution of WSS throughout the arterial system and found that superficial femoral artery had the lowest mean and peak WSS (see Table 2).

TABLE 2. Mean WSS [Pa] in the arteries ($\mu = 0.004\,\mathrm{Pa\,s}$).

Artery	WSS measured by Wu et al.	WSS predicted using the data by Wu et al.
Brachial	0.49 ± 0.25	0.42
Common carotid	0.83 ± 0.15	1.043
Femoral	0.33 ± 0.15	0.306

This can be explained once the difference between the diameters of the arteries in our model and their work is taken into account. When the mean diameters reported in [26] were used in our model, good agreement was found between the simulation and the measurements: the values for WSS in common carotid artery were found to be within 20% of each other, for mean WSS in femoral artery they were found to be within 7% of each other, and for mean WSS in brachial artery they were found to be within 14% of each other(no other parameters had been changed). This shows that flow and dia-

meter changes have significant influence on WSS values, which is consistent with the findings of Box et al. [3].

It is well known that arteries adapt to long-term increases or decreases in WSS, so if the flow rate is altered from its physiologic state for a long period, the arterial diameter changes to recover the physiologic range of shear in the range 1–2 Pa [28, 9, 8]. In our work remodelling of the artery walls was not taken into account. Our model predicts non-uniform distribution of WSS in the arterial tree. However, we cannot definitely state whether it is the case or simply a result of using the model parameters, which are incorrect. More work is required to validate the model parameters.

Limitations of our model due to its linearity were extensively discussed earlier [1, 13, 18]. It was reported that nonlinearities present in the arterial system were in the order of 5–10% within physiological range of frequencies and pressures in the arterial system [19]. In this study we did not attempt to account for non-linear effects because fully developed flow was assumed to take place in the points of interest.

The methods used in our study can be employed to estimate WSS and oscillatory shear index [26] in order to determine which arteries are prone to disease in two ways:

1. Getting the velocity profiles as a function of flow rate rather than pressure gradient has an advantage: the flow waveforms recorded during conventional ultrasound diagnostics may be used as the input signal to estimate WSS at the points where the measurements are taken.

2. When the flow waveform from a particular artery is not available (or practically difficult to obtain), it can be synthesized with the aid of the model.

5. Conclusion

The 1D multi-branched model is easy to implement and it is not computationally demanding. In this work we used it to carry out a detailed quantitative analysis of the velocity profiles obtained by assigning specific values to the various distal portions of the multi-branched model of the human arterial tree. It has been shown that they have given physically realistic estimates of WSS at the different points of the system. It may therefore be a useful tool to estimate WSS in arteries, allowing the effect of alteration of model parameters on WSS to be investigated.

Acknowledgement

The authors would like to thank Prof. A. Avolio for his help. This study was funded by the Overseas Research Students Awards Scheme and EPSRC, whose generous support is gratefully acknowledged.

References

1. A. AVOLIO, *Multi-branched Model of the Human Arterial System*, Medical and Biological Engineering and Computing, **18**: 709–718, 1980.
2. A. AVOLIO, D. FA-QUAN, L. WEI-QIANG, L. YAO-FEI, H. ZHEN-JONG, X. LIAN-FEN, and M. O'ROURKE, *Effects of aging on arterial distensibility in populations with high and low prevalence of hypertension: comparison between urban and rural communities in China*, Circulation, **71**: 202–210, 1985.
3. F. BOX, R. VAN DER GEEST, M. RUTTEN, and J. REIBER, *The influence of flow, vessel diameter, and non-Newtonian blood viscosity on the wall shear stress in a carotid bifurcation model for unsteady flow*, Investigative Radiology, **40**(5): 277–294, 2005.
4. H. BUTCHER and W. NEWTON, *The influence of age, atherosclerosis and homotransplantation upon the elastic properties of major human arteries*, Annals of Surgery, **148**: 1–20, 1958.
5. C. CARO, *Alterations of arterial hemodynamics associated with risk factors for atherosclerosis and induced by pharmacological or physiologic means: implications for the development/management of atherosclerosis*, [in:] Hosoda, Yaginuma, Sugawara et al. [eds.] Recent Progress in Cardiovascular Mechanics, pp. 197–213, Switzerland, Harwood Academic Publishers, 1994.
6. C. CARO, T. PEDLEY, R. SCHROTER, and W. SEED, *The mechanics of the circulation*, p.53, Oxford University Press, 1978.
7. M. FRIEDMAN, O. DETERS, F. MARK, C. BARGERON, and G. HUTCHINS, *Arterial geometry affects hemodynamics—potential risk factor for atherosclerosis*, Atherosclerosis, **46**: 225–231, 1983.
8. D. GIDDENS, C. ZARINS, and S. GLAGOV, *The role of fluid mechanics in the localization and detection of atherosclerosis*, J. Biomech. Eng., **115**: 588–594, 1993.
9. S. GLAGOV, C. ZARINS, D. GIDDENS, and D. KU, *Hemodynamics and atherosclerosis: insights and perspectives gained from studies of human arteries*, Archives of Pathology Laboratory Medicine, **112**: 1018–1031, 1988.
10. S. GREENWALD, A. CARTER, and C. BERRY, *Effect of age on the in vitro reflection coefficient of the aortoiliac bifurcation in humans*, Circulation, **82**: 114–123, 1990.
11. T. IMURA, K. YAMAMOTO, K. KANAMORI, T. MIKAMI, and H. YASUDA, *Noninvasive ultrasonic measurement of the elastic properties of the human abdominal aorta*, Cardiovascular Research, **20**: 208–214, 1986.
12. M. KARAMANOGLU, E. GALLAGHER, A. AVOLIO, and M., O'ROURKE, *Functional origin of reflected pressure waves in a multibranched model of the human arterial system*, American Journal of Physiology, **267**: H1681–H1688, 1994.

13. M. KARAMANOGLU, E. GALLAGHER, A. AVOLIO, and M. O'ROURKE, *Pressure wave propagation in a multibranched model of the human upper limb*, American Journal of Physiology, **269**: H1363–H1369, 1995.

14. D. KU, D. GIDDENS, C. ZARINS, and S. GLAGOV, *Pulsatile flow and atherosclerosis in the human carotid bifurcation*, Arteriosclerosis, **5**: 293–302, 1985.

15. B. LEAROYD and M. TAYLOR, *Alterations with age in the visco-elastic properties of human arterial walls*, Circulation Research, **18**: 278–292, 1966.

16. Z. LIU, F. SHEN, and F. YIN, *Impedance of arterial system simulated by viscoelastic T tubes terminated in windkessels*, American J. Physiology, **256**: H1087–H1099, 1989.

17. T. NAKASHIMA, and J. TANIKAWA, *A study of human aortic distensibility with relation to atherosclerosis and aging*, Angiology, **22**: 477–490, 1971.

18. W. NICHOLS, M. O'ROURKE [eds.], *McDonald's blood flow in arteries. Theoretical, experimental and clinical principles*, 4$^{\text{th}}$ed., pp.104, 223–224, 240–242, Arnold 1998.

19. F. PYTHOUD, N. STERGIOPULOS, and J. MEISTER, *Separation of arterial pressure' waves into their forward and backward running components*, Journal of Biomechanical Engineering, **118**: 295–301, 1996.

20. P. SEGERS and P. VERDONCK, *Role of tapering in aortic wave reflection: hydraulic and mathematical model study*, Journal of Biomechanics, **33**: 299–306, 2000.

21. D. STEINMAN, *Image-based computational fluid dynamics modelling in realistic arterial geometries*, Annals of Biomedical Engineering, **30**: 483–497, 2002.

22. D. STEINMAN, D. VORP, C. ETHIER, *Computational modeling of arterial biomechanics: Insights into pathogenesis and treatment of vascular disease*, Journal of Vascular Surgery, **37**(5): 1118-1128, 2003.

23. C. TAYLOR, T. HUGHES, and C. ZARINS, *Finite element modeling of blood flow in arteries*, Comp. Methods in Appl. Mechanics and Engineering, **158**: 155–196, 1998.

24. D. VORP, D. STEINMAN, and C. ETHIER, *Computational modeling of arterial biomechanics*, Computing in Science and Engineering, **3**(5): 51–64, 2001.

25. J. WOMERSLEY, *Method for the calculation of velocity, rate of flow and viscous drag in arteries when the pressure gradient is known*, J. Physiology, **127**: 553–563, 1955.

26. S. WU, S. RINGGAARD, S. OYRE, M. HANSEN, S. RASMUS, and E. PEDERSEN, *Wall shear rates differ between the normal carotid, femoral, and brachial arteries: an in vivo MRI study*, Journal of Magnetic Resonance Imaging, **19**(2): 188–193, 2004.

27. C. ZARINS, D. GIDDENS, B. BHARADVAJ, V. SOTTIURAI, R. MABON, and S. GLAGOV, *Carotid bifurcation: quantitative correlation of plaque localization with flow velocity profiles and wall shear stress*, Circulation Research, **53**: 502–514, 1983.

28. C. ZARINS, M. ZATINA, D. GIDDENS, D. KU, and S. GLAGOV, *Shear stress regulations of artery lumen diameter in experimental atherogenesis*, Journal of Vascular Surgery, **5**: 413–420, 1987.